Liquid−Liquid Phase Separation in Mixed Organic/Inorganic Aerosol Particles

V. Gabriela Ciobanu,* Claudia Marcolli, Ulrich K. Krieger, Uwe Weers, and Thomas Peter

Institute for Atmospheric and Climate Science, ETH Zurich, Switzerland

Received: May 29, 2009; Revised Manuscript Received: August 26, 2009

Ⓦ **This paper contains enhanced objects available on the Internet at http://pubs.acs.org/JPCA.**

Currently, the physical state of mixed organic/inorganic aerosol particles is not well characterized, largely because of the still unclear chemical composition of the organic fraction and of its properties with respect to mixing with the inorganic fraction. To obtain insight in the possible phases and phase transitions of such aerosol particles, we investigated the ternary poly(ethylene glycol)-400/ammonium sulfate/water system as a representative model system with partially immiscible constituents. For this purpose, we used optical microscopy and micro-Raman spectroscopy on micrometer-sized particles deposited on a hydrophobically coated substrate. The particles show liquid−liquid phase separations both upon decreasing (∼90−85%) and increasing (during ammonium sulfate deliquescence) relative humidities. In dependence upon the organic-to-inorganic ratio, OIR (i.e., poly(ethylene glycol)-400 to ammonium sulfate dry mass), phase separation is observed to occur by fundamentally different mechanisms, namely, nucleation-and-growth (OIR = 8:1 to 2:1), spinodal decomposition (OIR = 1.5:1 to 1:1.5) and growth of a second phase at the surface of the particle (OIR = 1:2 to 1:8). For each of these mechanisms, after completion of the phase separation, the resulting morphology of the particles is an aqueous ammonium sulfate inner phase surrounded by a mainly poly(ethylene glycol)-400 containing outer phase. We depict the various physical states of the ternary system in the relative humidity/composition phase diagram, constructed from bulk data and single particle measurements. Given the complex chemical composition of the organic fraction in tropospheric aerosols, it is expected that repulsive forces between the organic and inorganic aerosol constituents exist and that liquid−liquid phase separations commonly occur. The presence of liquid−liquid phase separations may change the partitioning of semivolatile species between the gas and the condensed phase, whereas the predominantly organic shell is likely to influence heterogeneous chemical reactions, such as N_2O_5 hydrolysis.

1. Introduction

The physical state and structure of tropospheric aerosol particles is still largely unknown despite their importance for the aerosol radiative properties, for cloud formation, and for multiphase and heterogeneous chemistry in and on aerosol particles.[1] For example, optical properties of atmospheric aerosols are influenced by aerosol phases and particle morphology: owing their larger size, deliquesced particles scatter the solar radiation more effectively than solid ones.[2] Whether the aerosol particles are liquid or solid also affects heterogeneous and multiphase chemistry:[3] e.g., the hydrolysis of N_2O_5 was shown to proceed much faster on liquid particles than on solid ones.[4,5] Furthermore, a correct description of the aerosol phases is required for estimating the partitioning of semivolatile species between the gas and condensed phase.[6]

The physical state of an aerosol particle is determined by its chemical composition and its ability to supersaturate with respect to phase transitions, both in turn depending on chemical constituents, on relative humidity (RH) and on temperature.[7,8] Tropospheric aerosols are complex mixtures of inorganic salts such as ammonium sulfate and nitrate and organic substances. The organic material contributes ∼20−50% to the total fine aerosol mass at continental midlatitudes and as much as 90% in tropical forested areas.[9] An important fraction of the organic matter (∼20−70%) is water-soluble.[10,11] The organic aerosol fraction is expected to be present in liquid form even at low relative humidity (RH), because the very large number of organic compounds depresses the temperature at which solids form.[7] The inorganic salts may exhibit efflorescence (i.e., nucleation of a crystal followed by crystal growth and rapid loss of water) when RH decreases, and deliquescence (sudden water uptake with the formation of a saturated solution) when RH increases. Because of the energy barrier that has to be overcome for nucleation, the efflorescence relative humidity (ERH) of aerosol particles is usually significantly lower than the deliquescence relative humidity (DRH). The lifetime of tropospheric aerosol particles is typically a week before washout; therefore, the aerosol particles may experience several humidity cycles, which complicates the prediction of their physical state.[1]

In the presence of organics, the deliquescence and efflorescence of the inorganic components may remain almost constant or shift to lower values depending on the nature and mixing ratio of the constituents.[12−17] Efflorescence may even be totally suppressed. Therefore, the water-soluble organic fraction may extend the range of RH over which the aerosol particles are totally liquid.

The diverse chemical composition of the organic fraction complicates the characterization of the phases of mixed organic/inorganic aerosol particles. Depending whether attractive or repulsive interactions between organic and inorganic components prevail, water-soluble organics may be miscible with the inorganic constituents or form a separate phase within aerosol particles.[18−20] This behavior can be understood in terms of

* To whom correspondence should be addressed. Tel: +41-44-633-40-63. Fax: +41-44-633-10-58. E-mail: gabriela.ciobanu@env.ethz.ch.

10.1021/jp905054d CCC: $40.75
Published on Web 09/23/2009

salting-out and salting-in effects that result from organic−inorganic interactions. Salting-out interactions may also induce liquid−liquid phase separations during humidity cycles. Liquid−liquid phase separation has been observed in mixed organic/inorganic solutions consisting of polyols or poly(ethylene glycol)-400 (PEG-400) and salts such as NaCl and ammonium sulfate (AS).[18] Measurements of micrometer-sized particles levitated in an electrodynamic balance (EDB) consisting of PEG-400 and AS did, however, not provide direct evidence of liquid−liquid phase separation in such particles.[18]

In this study we have investigated PEG-400/AS micrometer-sized particles deposited on hydrophobically coated slides during hygroscopic cycles. This model system has been chosen due to the low vapor pressure of the organic component, representing a simplified system containing partly immiscible components and being at the same time suited for our experimental setup. PEG-400 has a typical molecular weight for HULIS[21,22] and is structurally similar to polyols, an important substance class that has been identified in aerosols.[10] The aim of this study is to gain more information on the kinetics of liquid−liquid phase separations and the resulting particle morphology.

The paper is structured as follows: the next section provides a short overview on liquid−liquid phase separations. The experimental setup used for characterizing the particles is described in the third section. The fourth section presents the sequence of phase changes for particles with different ratios of PEG-400 to AS and the identification of the observed phases, while the fifth section discusses the phase diagram of the PEG-400/AS/H_2O system and the morphologies of the particles. Section 6 undertakes a first step toward applying the findings to atmospheric aerosols and the final section presents the conclusions.

2. Basic Aspects of Liquid−Liquid Phase Separations

Liquid−liquid phase separation is an important process that has been investigated thoroughly for polymers, polymers and inorganic salt solutions,[23,24] glasses[25,26] and alloy systems.[27] Regarding the kinetics of liquid−liquid phase separation, two different mechanisms can be distinguished:

Nucleation-and-Growth Mechanism. A one-phase system that may eventually separate into two phases by nucleation-and-growth is metastable with respect to small fluctuations in concentration and can become unstable to large concentration fluctuations if these (1) are close to the concentration of the second phase and (2) have reached a critical amplitude and size (so-called critical nucleus).[25,28] For the formation of a critical nucleus an energy barrier has to be overcome. This process is usually described by classical nucleation theory using an Arrhenius-like expression to formulate the nucleation rate. Subcritical nuclei build up randomly within a system (liquid) and start to grow continuously once they have passed the critical size. Besides the energy released by converting from the metastable into the thermodynamically stable state (volume energy) and the energy consumed by having to form a new interface (surface energy), the nucleation is controlled by the energy barrier against diffusion of monomers and subcritical nuclei in the liquid phase while building the critical nucleus (diffusion activation energy). Also the growth process subsequent to nucleation is controlled by liquid phase diffusivity of the components to the interface regions, leading to a more or less complete demixing. Furthermore, growth of phase-separated regions by coalescence of these regions is possible. The surface tension will work to minimize their surface. Since both phases are liquids, spherical shapes minimize the surface for a fix volume. Therefore, it is expected that these regions have spherical shapes. Consequently, the morphology developed by the nucleation-and-growth mechanism consists of spherical droplets of the minor phase dispersed in the major phase.

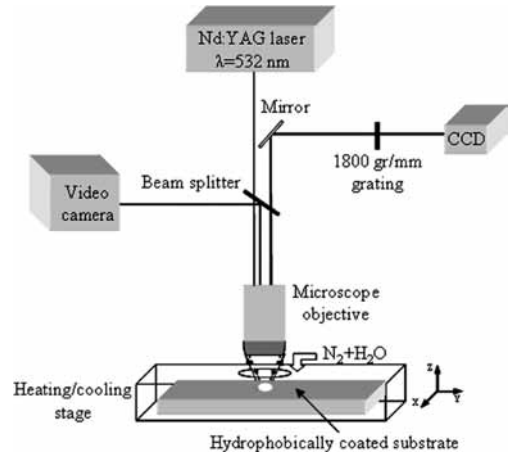

Figure 1. Schematic representation of the experimental setup. The abbreviation gr/mm refers to grooves per millimeters.

Spinodal Decomposition. Besides the nucleation-and-growth mechanism, phase separation can involve spinodal decomposition with subsequent dispersed cluster growth and cluster aggregation (coalescence). In contrast to nucleation and growth, where an energy barrier has to be overcome to form nuclei of the second phase, spinodal decomposition occurs barrier-free and therefore throughout the liquid medium.[25,28] In this case the system has become unstable and concentration fluctuations of arbitrarily small amplitude suffice to induce phase separation without the need to overcome an energy barrier. As the demixing develops, the amplitude of fluctuations increases in time, causing changes in the composition of the two evolving phases until equilibrium compositions are reached. The ubiquitously occurring small separated regions are observable in the form of "schlieren". Spinodal decomposition differs from the nucleation-and-growth mechanism by the fact that the first occurs throughout the whole solution volume as a concerted process, whereas nucleation takes place in just a few nucleation centers.[26] The morphological structure expected for the earliest stage of spinodal decomposition consists of highly interconnected phases—the schlieren—which will change gradually in time until an equilibrium arrangement is reached.

3. Experimental Section

There are a number of observational techniques allowing us to detect and distinguish the nucleation-and-growth mechanism and the spinodal decomposition in transparent media. These comprise optical microscopy,[29] scattering techniques such as phase contrast optical microscopy and polarized light microscopy,[30] schlieren visualization as a highly sensitive method based on the deflection of light by refractive index gradients,[31] all the way to more elaborate methods such as Raman microscopy.[32] The measurements reported on here rely on a combination of optical and Raman microscopy.

3.1. Experimental Setup. In the present work, single particle experiments were performed with a Raman microscope (Jobin Yvon, model: Labram) equipped with a heating/cooling cell (Linkam, model: LTS 120; see Figure 1) in which particles were deposited on a microscope slide mounted on the sample holder. The Raman system includes an external Nd:YAG laser (λ = 532 nm) as excitation source which was operated at 100 mW

power for illumination. The laser beam was fed into an Olympus microscope (BX-40). The backscattered light from the sample was analyzed by a spectrograph equipped with a grating (1800 grooves per millimeter) and a CCD detector. The Raman spectra were collected in the range from 150−4000 cm^{-1}, with a spectral resolution of ∼2−4 cm^{-1}. A black and white CCIR video camera with an acquisition frequency of 25 frames/s was used to acquire images and movies of the particles.

During the experiments, a constant temperature of 293.3 ± 0.1 K of the sample and in the gas volume was maintained by the cell's integrated Peltier elements below the sample holder and two additional Peltier elements mounted below the stage. A constant flow (∼130 sccm) of a N_2/H_2O mixture with a controlled H_2O partial pressure was pumped continuously through the cell. The water vapor mixing ratio of this flow was varied by changing the mixing ratio of a dry and a humidified nitrogen flow using automatic mass flow controllers. The humidified nitrogen flow was obtained by passing dry nitrogen over a temperature controlled water bath kept at 293 ± 0.01 K. The N_2/H_2O flow entered the cell through a ∼1 mm slit and was directed over the particle. A humidity sensor, with a capacitive thin film (Minicap2, Panametrics), was positioned in the stage ∼2 cm downstream of the particle. The sensor was calibrated inside the stage in response to varying water vapor mixing ratios of the humidified flow by changing the temperature of the humidifying water bath. The relative humidity was calculated as the ratio of the partial pressure of water vapor of the flow to the saturated vapor pressure of water at 293 K (the temperature inside the cell). The validity of the calibration curve was additionally confirmed by measuring the deliquescence relative humidity (DRH) of AS, NaCl, NH_4NO_3, and KNO_3 crystallites deposited on the microscope slide. The accuracy of the humidity sensor is ±1.5% RH. An Agilent VEE program was used for adjusting the mass flow controllers, readout of temperature and humidity, and the synchronization with the video signal. As most experiments were performed with a low rate of change of relative humidity (∼0.2% RH/min), the particle and the sensor were expected to react simultaneously to changes in relative humidity. Over longer time scales (weeks) the humidity sensor showed small drifts in the voltage values for a given relative humidity, which translated in significant offsets of relative humidity (up to 5% RH). Knowing from bulk measurements that the deliquescence of AS in the presence of PEG-400 is not changed,[18] the RH data from the humidity cycles were recalibrated frequently to the total deliquescence relative humidity of AS (DRH*), the deliquescence of AS in the ternary PEG-400/AS/H_2O system,[18] namely, DRH* = 80% or water activity $a_w = 0.8$ under equilibrium conditions (i.e., to the value observed for bulk measurements).

3.2. Materials. Aqueous solutions (with water activity $a_w >$ 0.9) containing different ratios of PEG-400 (Fluka, 91893) to AS (Fluka, 99.5%) were prepared using an analytical balance. Micrometer-sized droplets of the aqueous solutions were deposited on the microscope slide using a modified inkjet cartridge (Hewlett-Packard 51633 (a)) as droplet generator. The microscope slides were previously silanized (hydrophobically coated) by exposing them for 1 day to gaseous dimethyldichlorosilane. When the surface of the microscope slides is coated, the aqueous solutions form droplets on the microscope slide and heterogeneous nucleation due to surface contact is prevented. The coating procedure and the operation principle of the droplet generator have been described in detail in Knopf.[33]

3.3. Experimental Procedure. A typical experiment started with the preparation of an aqueous solution, followed by the deposition of few particles on a hydrophobically coated microscope slide using the droplet generator. One droplet was chosen and monitored with a long working distance objective (Olympus BX-40, magnification 50, aperture 0.7). At the beginning of the experiment the particle was equilibrated at high relative humidity (>90% RH). Subsequently, the relative humidity was decreased below the efflorescence relative humidity of AS and increased again to >90% RH. Optical images of the particles were recorded continuously during the experiment on an HD recorder and evaluated afterward. Raman spectra were collected during the experiments to identify the chemical composition of the liquid and solid phases of the particle. To obtain spectra with a better signal-to-noise ratio, the particles were equilibrated at relative humidities at which no phase transition was expected and spectra were recorded for ∼15 min.

4. Results

To establish the influence of the organic fraction on the AS phase changes, we investigated single particles containing a number of organic-to-inorganic ratios (OIR, expressed as PEG-400/AS dry mass ratio) ranging from OIR = 1:8 to 8:1. In the following, we present in detail the results for particles with OIR = 1:1, 8:1, and 1:2, and briefly refer to other ratios with similar behavior.

4.1. PEG-400/AS, 1:1 (by Weight). Figure 2a shows images of a ∼31 μm (dry diameter) particle containing PEG-400/AS in equal masses (OIR = 1:1) at different times while the relative humidity is reduced from RH ≈ 93.1% to 4.4% at a rate of $dRH/dt = -0.2\%$/min. At RH ≥ 89.7% the droplet displays only one liquid phase. Time 0 represents the first onset of phase transition. Phase separation occurs at RH ≈ 89.7%, when the appearance of schlieren (Figure 2a, $t = 3$ s) is observed. The schlieren develop into spherical droplets ($t = 6$ s), which coalesce to form the inner phase of the particle. At RH ≈ 89.5% two clearly delimited liquid phases inside the particle can be observed. The chemical composition of the liquid phases was determined from Raman spectra (see section 4.4). The inner phase is aqueous AS and the outer phase aqueous PEG-400 (and this arrangement is observed not only in the case depicted here but also in all investigated droplets). The satellite inclusions observed in the outer liquid phase were spectroscopically identified as being aqueous AS. A further decrease in RH leads to the shrinkage of the particle due to water evaporation and to a decrease in the number of satellite AS inclusions because they coalesce with the inner AS phase. Both developments can be seen in Figure 2a by comparing the particle's images at RH ≈ 89.5% and 49%. At RH ≈ 35% AS effloresces while PEG-400 remains liquid, forming an outer phase consisting mainly of PEG-400 with small contributions of water and AS. Some PEG-400 is also found to be trapped in the crystal. A movie showing the changes of particle phases during drying conditions is available (see Appendix B).

Upon subsequent moistening, liquid−liquid phase separation develops when AS deliquesces, i.e., during deliquescence the particle consists of the remnants of the solid (AS) plus two liquid phases. When all AS has deliquesced, the two liquid phases are distributed as in Figure 2a, $t = 16$ s, except that there are no satellite inclusions in the outer phase. A further increase in RH results in the restoration of one liquid phase at RH ≈ 89.5%.

Similar behavior was observed for other particles in the size range 14−67 μm dry diameter. The phase changes occur at RH comparable to those shown in Figure 2 for 31 μm (phase separation upon drying between 88 and 90.3% RH, AS efflorescence between 28.9 and 41.5% RH and one liquid phase

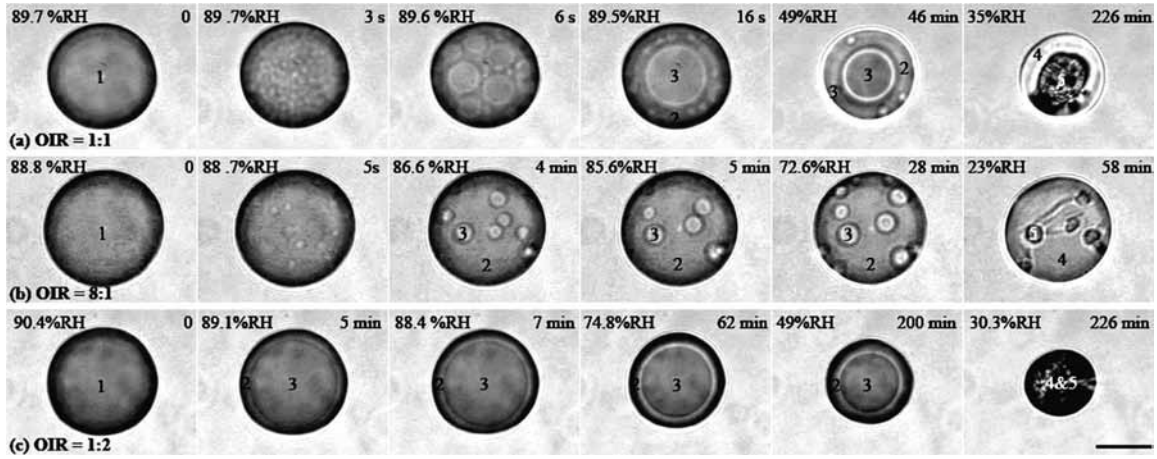

Figure 2. Morphologies of PEG-400/AS particles at different times and different relative humidities (RH). Organic-to-inorganic dry mass ratios (OIR) of PEG-400/AS are (a) 1:1, (b) 8:1, and (c) 1:2. Small numbers on particle regions indicate compositions of phases: 1, aqueous solution of PEG-400 and AS; 2, aqueous PEG-400; 3, aqueous AS; 4, mainly PEG-400 (with small contributions of water and AS); 5, crystallized AS. The length bar in the rightmost lower figure corresponds to 20 μm and applies to all 18 images. For comparison with the movies see Appendix B.

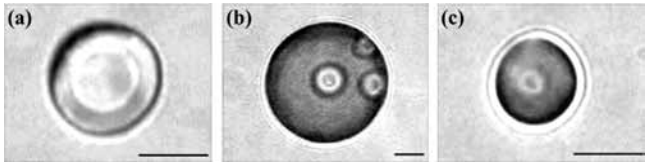

Figure 3. Morphology of PEG-400/AS particles upon moistening directly following AS deliquescence: (a) 1:1 ratio; (b) and (c) 8:1 ratios of PEG-400/AS. The bars indicate 10 μm in each panel. In panel c the particle is out of focus and consequently the outer ring is observed.

formation between 88.1 and 89.6% RH). However, the smaller droplets had fewer or no aqueous AS satellite inclusions imbedded in the PEG-400 rich shell (e.g., the 17 μm particle in Figure 3a). Particles with OIR = 1.5:1, 1.2:1, 1:1.2, and 1:1.5 behave in the same manner as the 1:1 mixtures, the only difference being the thickness of the outer phase (thicker for particles with OIR = 1.5:1 and 1.2:1 and thinner for particles with 1:1.2 and 1:1.5).

4.2. PEG-400/AS, 8:1 (by Weight). The behavior of organic-rich particles with OIR = 8:1 (PEG-400/AS of dry mass) exposed to decreasing RH is illustrated in Figure 2b. A rate of $dRH/dt \approx -1\%$/min was used for this experiment. While at high RH the particle is present as one single liquid phase as in the preceding case, phase separation occurs for this composition by the consecutive formation of a finite number of isolated small inclusions at RH $\approx$ 88.7% randomly scattered throughout the particle. These inclusions grow in time; some of them coalesce and form larger inclusions. Upon decreasing the RH, these inclusions coalesce to RH $\approx$ 85.3% but continue to be generated by nucleation from the mixed liquid to RH $\approx$ 80.7%. Their chemical composition was identified by micro-Raman spectroscopy as mainly aqueous AS, while the major phase surrounding them is aqueous PEG-400. As the AS remains distributed as aqueous AS inclusions in the volume of the particle, we observe a stepwise efflorescence in the range 27−23% RH. At the beginning, some AS inclusions crystallize. Needles grow from the resulting crystals and seed crystallization of other aqueous AS inclusions. Other inclusions disappear without crystallizing, presumably because AS diffuses from these inclusions to the crystallized AS along the concentration gradients in the organic particle's phase. The morphology of the particle with completely effloresced AS is presented in Figure 2b at t = 58 min.

For subsequently increasing RH, AS deliquescence occurs at RH $\approx$ 80%. As some AS crystals remained isolated after the efflorescence (no needles connecting them), separated AS droplets form after deliquescence (Figure 3b) in contrast to the case with OIR = 1:1. Only at RH $\geq$ 87% does the droplet again convert into a single liquid phase. A movie showing the changes of particle phases during drying and humidifying conditions is available (see Appendix B).

Similar behavior was observed for particles in the size range 12−61 μm dry diameter. Again, a decrease in the size of the particle leads to a decrease in the number of AS inclusions (just one remaining for a particle with 12 μm dry diameter, Figure 3c). On the other hand, an increase of the number of aqueous AS inclusions and of their coalescence events is observed when increasing OIR (e.g., for OIR = 2:1). The morphology of the separated phases for OIR = 2:1 resembles that observed of OIR = 1:1, see t = 46 min in Figure 2a despite the different separation mechanism.

4.3. PEG-400/AS, 1:2 (by Weight). Figure 2c shows the morphologies of a PEG-400/AS particle with OIR = 1:2 (by weight) at different times and RH. As in the previous cases, at high relative humidity, the particle consists of one liquid phase. Decreasing relative humidity leads to liquid−liquid phase separation at RH $\approx$ 89.7%. In this case the organic-rich phase is observed to grow immediately as a shell from the liquid−gas interface, surrounding the aqueous AS core (Figure 2c, t = 5 min). A further decrease in RH leads to shrinkage of the particle and an apparent increase in the thickness of the PEG-400 phase. After AS effloresced (at RH $\approx$ 30.3%), the PEG-400 phase can no longer be microscopically distinguished from the solid AS. Raman spectra collected at different points of the particle reveal weak band of PEG-400 suggesting that the liquid PEG-400 is trapped within the crystalline phase. A movie showing the changes of particle phases during drying conditions is available (see Appendix B).

Upon subsequent moistening, the particle follows the same route as observed for the OIR = 1:1 particles. Two liquid phases form during the AS deliquescence and merge into one liquid phase when RH $\geq$ 89.3%. Similar phase changes have been observed for particles in the size range 16−38 μm dry diameter. For particles with OIR = 1:4 and 1:8 the phase separation was not always clearly detectable. In contrast to the 1:2 case where the interface between the PEG-rich shell and AS-core was detectable as a sharp ring, for particles with 1:4 and 1:8 ratios of PEG-400/AS only an incomplete ring was observed, probably

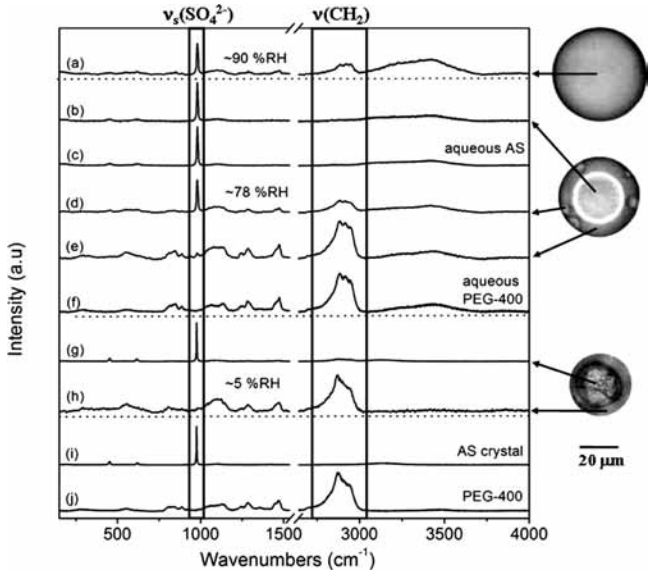

Figure 4. Raman spectra and microscopy images of a droplet with organic-to-inorganic ratio OIR = 1:1 (PEG-400/AS dry mass ratio) at RH ≈ 90% (a), 78% ((b), (d), and (e)) and 5% ((g) and (h)). For comparison, spectrum c shows an aqueous AS and spectrum f an aqueous PEG-400 droplet at RH ≈ 78%. Spectra i and j show pure AS and pure PEG-400, respectively. All spectra cover 150−4000 cm^{-1} and are vertically shifted for a better visibility. The dotted lines separate regions with different relative humidity. Length bar indicates 20 μm applying to all three particle images.

due to lack of contrast resulting from the thinner PEG-rich shell in the microscopic images.

4.4. Raman Spectra of 1:1 (by Weight) PEG-400/AS Particles. Representative Raman spectra and microscopy images collected from a particle with OIR = 1:1 at RH ≈ 90%, 78%, and 5% are shown in Figure 4. The Raman spectra provide information on the chemical composition of the particle's liquid and solid phases as well as on the mixing of components. The assignments of the PEG-400 peaks was done according to Di Noto et al.[34] and Matsuura and Miyazawa,[35] those of AS and H_2O according to Dong et al.[36] and Colberg[37] as reported in Table 1.

The main features of spectrum a, collected at RH ≈ 90%, are the sharp peak at ~981 cm^{-1} and the broad band between ~2785 and ~3016 cm^{-1}, which correspond to the symmetric stretching mode of SO_4^{2-} and to the C−H stretching vibrations of PEG-400, respectively. They provide clear evidence for the presence of both AS and PEG-400 in one liquid phase. The additional broad band in the range ~3020−3710 cm^{-1} is due to the symmetric and antisymmetric O−H stretching modes of water molecules. A decrease in relative humidity leads to the formation of two liquid phases and a decrease in the intensity of the water band indicative of water evaporation.

At RH ≈ 78% Raman spectra were collected from the inner and outer phases, as well as from the satellite inclusions of the outer phase. Spectrum b collected from the inner liquid phase presents a spectral signature similar to that of an aqueous AS solution as in spectrum c (see also Dong et al.[36]). Besides the intense band at ~981 cm^{-1}, the SO_4^{2-} antisymmetric stretching mode at ~1100 cm^{-1}, and the bending modes at ~452 and ~617 cm^{-1}, can be distinguished in the spectrum. The positions of these peaks are similar to those of an aqueous AS particle at RH ≈ 78%, which we also determined with the present experimental setup (see Table 1).

Spectrum d acquired from a satellite inclusion suggests the presence of both AS and PEG-400 spectral signatures. However,

TABLE 1: Molecular Vibration Assignments of the PEG-400/AS/H_2O System

compound	wavenumber in cm^{-1} and intensity[a,b]										ref ν (cm^{-1})	assignment[c]
	(a)	(b)	(c)	(d)	(e)	(f)	(g)	(h)	(i)	(j)		
ammonium sulfate	450 (w)	452 (w)	453 (w)	453 (w)			452 (w)		451 (w)		452[d] (36), 451[e] (36)	δ_s (SO_4^{2-})
	618 (w)	617 (w)	620 (w)	618 (w)			617 (w)		619 (w)		615[d] (37), 612[e] (36)	δ_{as}(SO_4^{2-})
	981 (vs)	981 (vs)	981 (vs)	980 (vs)	982 (w)		977 (vs)		976 (vs)		981[d] (36), 979.9[d] (36), 976[e] (37), 975[e] (36)	ν_s(SO_4^{2-})
		1102 (w)	1102 (w)				1080 (w)		1100 (w)		1104[d] (36)	ν_{as}(SO_4^{2-})
							3132 (w)		3141 (w)		3136[e] (36)	ν_{as}(NH_4^+)
poly(ethylene glycol)-400	553 (w)			553 (w)	555 (w)	557 (w)		553 (m)		552 (w)	536 (34), 537 (35)	δ(CCO), δ(COC), r(CH_2)
	836 (w)			837 (w)	833 (w)	832 (w)		821 (w)		829 (w)	830 (34), 846 (35)	r(CH_2), ν(CO)
	889 (w)				888 (w)	890 (w)		887 (w)		892 (w)	880 (34)	ν(CO), r(CH_2)
	1122 (m)			1115 (w)	1128 (m)	1134 (m)	1136 (w)	1110 (m)		1134 (m)	1130 (34), 1143 (35)	ν(CO), r(CH_2)
	1251 (w)			1247 (w)	1245 (w)	1242 (m)	1242 (w)	1247 (w)		1243 (m)	1243 (34), 1235 (35)	t(CH_2)
	1289 (w)			1286 (w)	1286 (w)	1289 (w)	1289 (w)	1286 (w)		1288 (w)	1283 (34), 1282 (35)	t(CH_2)
	1466 (w)			1465 (w)	1466 (m)	1463 (m)	1462 (w)	1464 (w)		1464 (m)	1464 (34)	sr(CH_2)
	2894 (m, b)			2887 (s, b)	2888 (s, b)	2885 (s, b)	2875 (w, b)	2877 (s, b)		2874 (s)	2869 (34), 2890 (35)	ν_s(CH_2)
	2953 (m, b)			2953 (s, b)	2951 (s, b)	2949 (s, b)	2941 (w, b)	2944 (s, b)		2944 (s)	2932 (34), 2939 (35)	ν_{as}(CH_2)
water	3212 (s, b)	3160 (m, b)	3147 (m,b)	3214 (m, b)	3248 (w, b)	3255 (m, b)					3248 (36)	ν_s(OH)
	3430 (s, b)	3427 (m, b)	3422 (m,b)	3443 (m, b)	3440 (w, b)	3443 (m, b)					3468 (36)	ν_{as}(OH)

[a] (a) PEG-400/AS particle at 90% RH; (b), (d), (e) PEG-400/AS particle at 78% RH; (c) aqueous AS solution; (f) aqueous PEG-400 solution; (g), (h) PEG-400/AS particle at 5% RH; (i) AS crystal; (j) pure PEG-400. [b] vs: very strong. s: strong. m: medium. w: weak. b: broad. [c] ν: stretching. δ: bending; r: rocking. t: twisting. sr: scissoring. as: antisymmetric mode. s: symmetric mode. [d] Aqueous AS solution. [e] Solid AS.

on the basis of the physical behavior of these inclusions—namely, coalescence with the inner phase and crystallization—they should actually have the same composition as the inner phase. It is most likely that PEG molecules of the outer phase contribute to the Raman measurement of the satellite inclusions, because these are relatively small and surrounded by the PEG-400 phase, which is traversed by the laser light during the measurement. While this interpretation is sensible, we cannot exclude that small amounts of PEG-400 may be present within the satellite inclusions.

The outer liquid phase was found to be mainly aqueous PEG-400, most of the peaks belonging to the PEG vibration modes; see spectrum e and compare with spectrum f taken from an aqueous PEG-400 droplet. The $\nu_s(SO_4^{2-})$ band at ~982 cm^{-1} appears in spectrum e, but with a very low intensity, indicative of a low concentration of AS ions in the PEG-400 rich phase.

At RH ≈ 5% the spectrum g collected from the inner phase shows a shift for the $\nu_s(SO_4^{2-})$ band from 981 cm^{-1} (at ~90% RH) to 977 cm^{-1} (at ~5% RH), which is in agreement with a previous study that showed such a shift for crystalline AS compared with the aqueous solution, from 979.9 to 975 cm^{-1}.[36] The band corresponding to the C−H stretching mode of PEG-400 is also present in spectrum g, which could be either due to PEG-400 molecules of the outer phase (as in the case of satellite inclusions) or from cavities with liquid PEG-400 embedded within the AS crystalline matrix. Spectrum h of the liquid phase surrounding the effloresced AS shows the same spectral features as spectrum e for RH ≈ 78%, except that the $\nu_s(SO_4^{2-})$ peak and the water band are no longer visible. Spectrum h is also similar to spectrum j acquired from pure PEG-400. Similar spectral features have been observed for ratios of PEG-400/AS of 8:1 and 1:2, only with differences in the relative AS/PEG-400 band intensities.

5. Discussion

5.1. Phase Diagram of PEG-400/AS/H_2O System. The bulk data together with the results of single particle measurements are used to construct a combined RH/composition equilibrium and metastability phase diagram[38] of the PEG-400/AS/H_2O ternary system (see Figure 5). The lower abscissa shows the AS dry mass fraction, x_{AS}, as weighed in during solution preparation, while the upper abscissa shows the organic-to-inorganic ratio OIR = $(1 - x_{AS})/x_{AS}$. The particulate water fraction in the particles depends on RH and cannot be directly derived with this setup. Three lines separate different regions of the phase diagram: the AS efflorescence line, the two-liquid-phases line, and the two-liquid-phases/one-liquid-phase boundary.

Bulk Measurements. The two-liquid-phases line and the two-liquid-phases/one-liquid-phase boundary were both established by Marcolli and Krieger[18] and represent thermodynamic equilibrium. At the two-liquid-phases line both liquid phases are saturated with respect to AS. Above the two-liquid-phases line, the stable state of the system is two liquid phases up to the two-liquid-phases/one-liquid-phase boundary, above which the two liquid phases merge into one liquid phase. The one-liquid-phase region for the mixed PEG-400/AS is larger than, for example, the one-liquid-phase region of PEG-1540/AS and PEG-4000/AS systems (see Albertsson[23]). In bulk measurements efflorescence is triggered by heterogeneous nucleation; therefore, single particle measurements are required to determine ERH.

Single Particle Measurements. During the humidity cycles performed on single particles, the following phase transitions are observed upon drying: one liquid phase is followed by two liquid phases, and next by one liquid and one solid phase. Upon moistening, the same phase states are passed, but in reverse order. The deliquescence of AS and the formation of two liquid phases occur within the whole composition range at almost the same relative humidity. Since we use the AS DRH* values as recalibration points for the humidity sensor (DRH* = 80%, corresponding to a water activity $a_w = 0.8$), they perfectly match the two-liquid-phases line. The points indicating the beginning of AS deliquescence (solid circles in Figure 5) are determined by eye, namely, the RH at which the AS crystal starts to dissolve partly (with a concomitant uptake of a small amount of water), causing a noticeable change in its morphology without significant growth of particle size. The water activity at which one liquid phase forms shows a slightly stronger dependence on the PEG-400/AS ratio. The RH at which one liquid phase forms in micrometer-sized particles upon moistening, coincides with the two-liquid-phases/one-liquid-phase boundary observed in bulk solutions. Upon drying, liquid−liquid phase separation occurs at the two-liquid-phases/one-liquid-phase boundary. The lack of difference between the bulk and single particle measurements suggests that liquid−liquid phase separation in this system occurs at low or even negligible supersaturations.

In single particle measurements the state of the system between the AS efflorescence and two-liquid-phases lines depends on the humidity history. Upon drying, the system remains in the two-liquid-phases state until AS effloresces, while upon moistening, one liquid phase (mainly PEG-400) and one solid phase (crystalline AS) coexist until AS deliquesces. Below

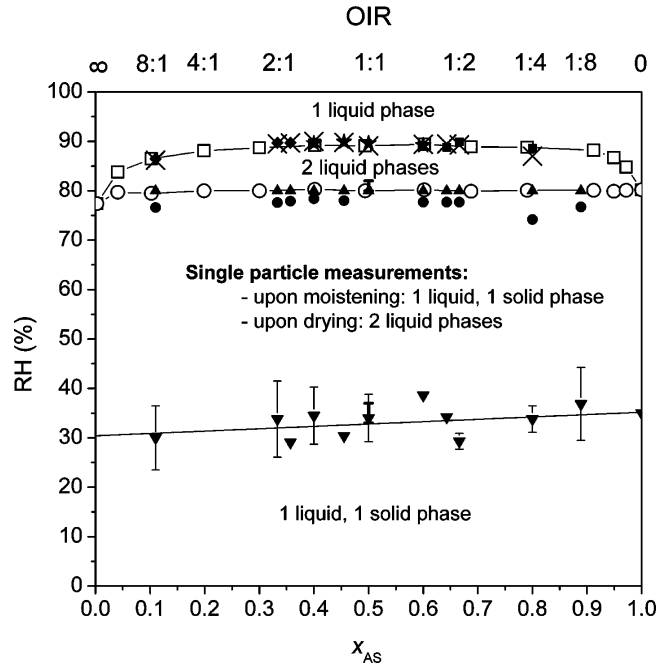

Figure 5. RH/composition equilibrium and metastability phase diagram of the PEG-400/AS/H_2O ternary system. Lower abscissa: AS dry mass fraction x_{AS}. Upper abscissa: organic-to-inorganic ratio OIR = $(1 - x_{AS})/x_{AS}$. Open symbols indicate bulk measurements: ○, two-liquid-phases line; □, two-liquid-phases/one-liquid-phase boundary. Solid symbols indicate particle measurements. Upon drying: ◆, one-liquid-phase/two-liquid-phases by nucleation-and-growth; ★, one-liquid-phase/two-liquid-phases by spinodal decomposition; ■, one-liquid phase/two-liquid-phases by growth of the second phase from the surface; ▼, AS efflorescence (the thin error bars represent the standard deviation for the AS ERH). Upon moistening: ●, beginning of AS deliquescence; ▲, AS totally deliquesced/two-liquid-phases; ×, two-liquid-phases/one-liquid-phase (partly hidden by solid symbols). EDB measurements from Marcolli and Krieger:[18] **I** AS efflorescence and deliquescence ranges (the thick bars give the range of AS DRHs and ERHs observed with the EDB).

the AS efflorescence line the system is always present as one liquid (mainly PEG-400) and one solid (crystalline AS) phase. The large hysteresis between AS deliquescence and efflorescence indicates that a high supersaturation is needed to overcome the AS nucleation threshold. The values observed for AS efflorescence (ERH = 18.9−43.5% are in the same range or even lower than the ones observed in EDB experiments that have been performed on micrometer-sized PEG-400/AS particles (1:1 ratio by weight) (33−37% RH).[18] ERH shows a considerable scatter due to the stochastic nature of the nucleation process, with a similar range as the one for pure AS particles (ERH = 33−48%, Martin and the references therein[2]).

5.2. Liquid−Liquid Phase Separation Mechanisms Identified for the PEG-400/AS/H_2O System. As indicated in Figure 5, liquid−liquid phase separation occurs upon drying at the two-liquid-phases/one-liquid-phase boundary. The phase separation mechanisms are identified according to the morphologies developed at the onset of phase separation or during the growth of the second phase. In the Results we showed that phase separation occurred either via the formation of AS inclusions (OIR = 8:1 to 2:1) or via the formation of schlieren, which develop into AS inclusions upon coalescence (OIR = 1.5:1 to 1:1.5), or finally by the growth of a second PEG-rich phase from the particle's rim (OIR = 1:2 to 1:8).

In the following we use the chronological sequence of appearance of the inclusions to substantiate our understanding of the processes responsible for the observed phase separation. Figure 6 illustrates the differences in the evolution of the number of AS inclusions in dependence upon the organic-to-inorganic ratio OIR. For OIR = 8:1 (Figure 6a) the inclusion number increases over a time period of several minutes, followed by a decrease due to coalescence. The lack of interconnectivity between aqueous AS inclusions and the increase of their number in time are typical for a nucleation-and-growth mechanism. Similar behavior is observed for OIR = 2:1 (Figure 6b), but for this ratio a larger number of nucleation and coalescence events takes place, as one might have expected from the higher abundance of AS.

Conversely, in the case of OIR = 1:1 there is a high interconnectivity of the PEG-400 and AS phases observed at the onset of phase separation, which is indicative of spinodal decomposition (Figure 7). The phase separation occurs in a concerted process yielding a high number of aqueous AS inclusions, which coalesce within less than a minute (Figure 6c) to form a main aqueous AS inner phase surrounded by satellite inclusions in the case of larger particles. The large number of individual domains (schlieren), and their high degree of interconnectivity, their rapid appearance, merging and fluctuating decomposition renders a quantification of their number during the earliest stages of phase separation impossible. Also, this initial number may well be limited by the resolution of our microscopic setup. However, if the spinodal decomposition develops into droplets of the second phase in a continuous first phase, discrimination between nucleation and growth and spinodal decomposition can become ambiguous unless the first stage of phase separation can be visually resolved.

5.3. Particle Morphology. There are several factors contributing to the observed morphologies of mixed PEG-400/AS particles at different RHs. These will be addressed in the following.

Considerations of Surface Tension. For PEG-400/AS particles consisting of two liquid phases, the outer phase was always the PEG-rich phase. This behavior is in accordance with considerations of surface tension: PEG-400 has a lower surface tension (44.5 mN/m)[18] than aqueous AS solutions (88.8 mN/m at $a_w = 0.8$).[39] The equilibrium shape (morphology) of a droplet containing two immiscible liquids will strive to assume a

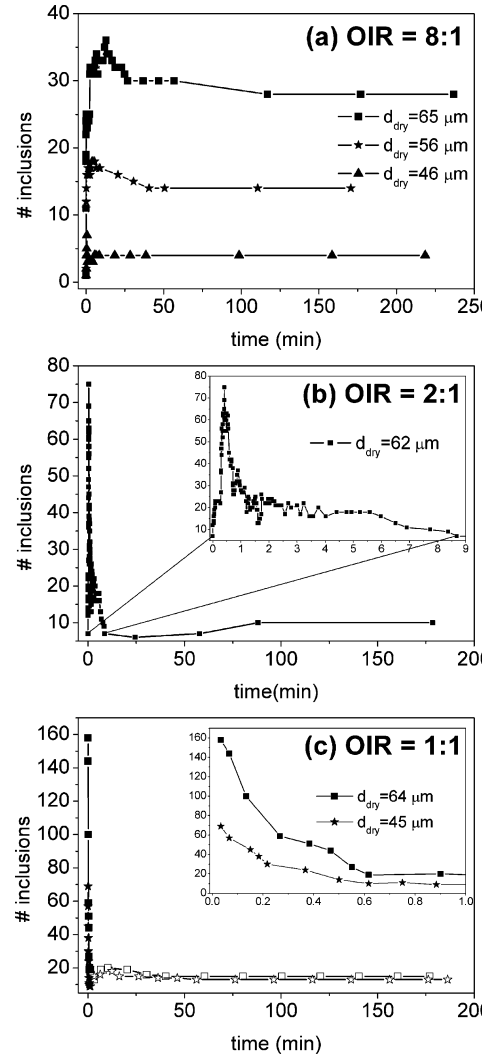

Figure 6. Evolution of the number of aqueous AS inclusions as a function of time: (a) OIR = 8:1; (b) OIR = 2:1; (c) OIR = 1:1. Time 0 corresponds to the onset of phase separation. The solid lines are to guide the eye. Panel c: solid lines start at 2 s for both particle sizes, when the number of AS inclusions has become countable (counting of AS inclusions is uncertain because of still present interconnectivity): solid symbols, total number of inclusions, whose evolution during the first minute of phase separation is given in the inset; open symbols, number of AS satellite inclusions that are present in the outer PEG-400 phase after the inner AS phase has formed.

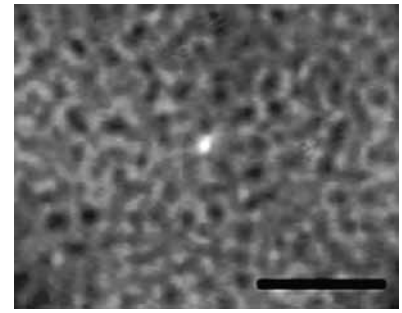

Figure 7. Snapshot taken at the beginning of phase separation of a 1:1 PEG-400/AS particle at t = 2s (first frame), illustrating the interconnectivity between the two liquid phases (schlieren texture). The length bar in the figure represents 20 μm.

minimum surface energy.[40] For liquids that are wetting each other, this is achieved when the liquid with lower surface tension is at the surface[27] and covers uniformly the inner phase.

Diffusion of AS Inclusions within the PEG-400 Phase. The number of AS inclusions in the PEG-400 phase (outer phase or major phase) was found to depend on the size of the entire particles. Figure 8a shows a decrease of the number of AS satellite inclusions in the outer phase with decreasing the size of particles with OIR = 1:1, while in Figure 8b a similar behavior is shown for the AS inclusions in the major phase for particles with OIR = 8:1. In both cases diffusion of the AS ions (NH_4^+ and SO_4^{2-}) to the inclusions limits the growth of AS inclusions in a first stage, and the diffusion of the AS inclusions themselves to the inner phase (for OIR = 1:1) or to other AS inclusions (for OIR = 8:1) limits the growth in a later stage. Since the ion mobility is much higher than that of the inclusions, the later growth stage is the overall time-limiting step. In the following we estimate the characteristic times for these diffusion processes.

The characteristic times for diffusion of AS ions or inclusions within a liquid phase particle and hence for the absorption of the ions or the collision and coalescence of the inclusions is given by

$$\tau = \frac{x^2}{6D_l} \tag{1}$$

where x is the typical distance between the ions and an inclusion or between two inclusions (either between two satellite inclusions or between a satellite and the central inclusion) and D_l is the liquid phase diffusion coefficient.[41] The characteristic time for diffusion of AS ions at the onset of phase separation (water is the predominant component at high RH) along a distance x = 0.1 × radius of the particle is estimated to be 0.7 ms (e.g., for a 20 μm radius particle), when assuming $D_l \sim 10^{-5}$ cm^2/s approximated from D_l of AS in aqueous solutions.[42] This short time may explain the observed fast initial growth of AS inclusions at high RH.

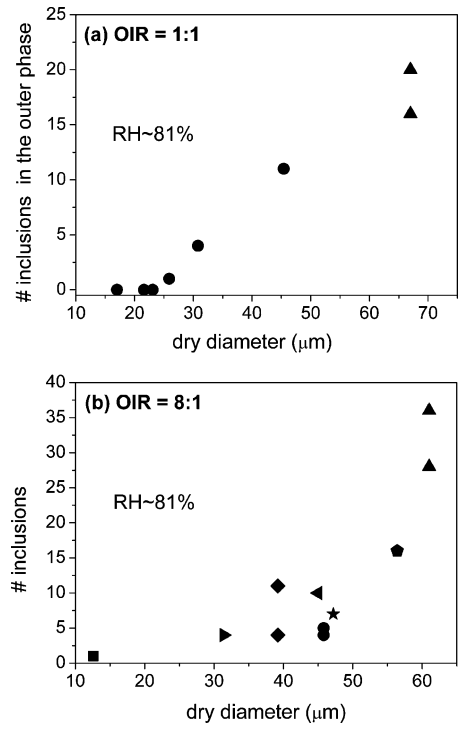

Figure 8. Number of aqueous AS inclusions as a function of particle size: (a) AS inclusions in the outer phase of particles with OIR = 1:1; (b) AS inclusions in the volume of particles with OIR = 8:1. The same type of symbol is used to represent data obtained for the same particle during different drying cycles.

The diffusion of AS inclusions in PEG-400 is much slower. Their diffusion coefficient can be estimated by means of the Stokes−Einstein relationship, which reads[43]

$$D_{incl} = \frac{k_B T}{6\pi\eta r_{AS}} \tag{2}$$

where k_B is the Boltzmann constant, T is the temperature, η the viscosity of the medium, and r_{AS} is the radius of AS inclusion (approximated here as a spherical particle).

As aforementioned, two cases are distinguished for the diffusion of AS inclusions: (a) diffusion of AS satellite inclusions to the inner aqueous AS phase and (b) diffusion of AS inclusions toward each other in the PEG-400 phase.

(a) Diffusion of AS Inclusions to the Inner Aqueous AS Phase. The AS inclusions in the PEG-400 outer phase for particles with OIR = 1:1 are the result of spinodal decomposition and coalescence of AS regions during the initial stage of phase separation. The characteristic time for diffusion of these inclusions to the inner phase can be estimated using eq 1, where x represents in this case the distance between the satellite inclusions and the inner phase and the diffusion coefficient is given by eq 2. The sizes of AS inclusions are typically between $r_{AS} \sim 2$ and 3 μm and the viscosity of (water-free) PEG-400 is ~98 mPa·s,[44] which gives $D_{incl} \sim 10^{-11}$ cm^2/s. The characteristic time for diffusion for AS inclusions along $x \sim 4$ μm distance (e.g., Figure 2a) to the inner phase is $\tau \sim 45$ min. The estimated characteristic times are long owing to the high viscosity of PEG-400 and can explain why there is not much tendency of AS satellite inclusions to diffuse readily to the inner phase. The calculated characteristic time for the diffusion of AS satellite inclusions to the inner phase is in agreement with the time scale shown in Figure 6c, where hardly any change in the number of AS satellite inclusions (shown as open symbols) is observed after 40 and 56 min for the 64 and 45 μm diameter particles, respectively. However, a decrease in the number of AS satellite inclusions at shorter times occurred due to diffusion to the inner phase and/or coalescence with their neighbors. This can be explained by a lower viscosity of PEG-400 phase at high RH due to the water content.

(b) Diffusion of AS Inclusions toward Each Other in the PEG-400 Phase. For particles with OIR = 8:1 the formation of AS inclusions is initially the result of AS ions diffusing toward an earlier created nucleus. Later growth of AS inclusions occurs also by coalescence. The time required for two AS inclusions to diffuse to each other can be estimated by eq 1 but in this case x represents the minimum distance between two AS inclusions ranging between 2−14 μm (e.g., the situation shown in Figure 2b, t = 28 min). However, AS inclusions are also observed to be touching each other without coalescence. Either these inclusions may be situated in different planes inside the particle, so that their distance cannot be estimated microscopically, or they need to overcome an energy barrier to reduce their surface area by coalescence. The radius of AS inclusions and consequently D_{incl} are the same as in the previous case ($r_{AS} \sim 2$ to 3 μm and $D_{incl} \sim 10^{-11}$ cm^2/s) which gives a characteristic time for diffusion of $\tau \sim 11$ min and ~ 9 h for a distance of 2 and 14 μm, respectively. Indeed, the estimated τ's are of the

same order as the time for decimation of inclusions in Figure 6a. The particles shown in Figure 2a,b show therefore more than one AS inclusion. The increased number of coalescence events immediately after phase separation, may be explained by the lower viscosity of the major phase at high RH (when water represents an important fraction of particle mass). As RH is decreased, the viscosity of the major phase approaches the one of pure PEG-400, which impedes the movement of AS inclusions to each other, and consequently the number of AS inclusions remains constant up to AS efflorescence.

6. Potential Implications for the Atmosphere

The PEG-400/AS particles investigated in this study can be considered as representing mixed organic/sulfate particles that dominate the aerosol in the accumulation mode in large parts of the troposphere. The organic component may represent the aged organic fraction, which is likely to be water-soluble, with a rather low concentration of surfactants. Solutions containing such organics are likely to show liquid−liquid phase separation at low RH in the presence of inorganic salts, but are completely miscible at high RH.[18] To what degree such phase separations occur in natural aerosol particles and what the resulting morphology is depends on the kinetics of phase separation. Particles in this study were much larger than accumulation mode particles and were deposited on a substrate instead of freely suspended in the air. Nevertheless, by scaling to the submicrometereter size range we will speculate on how our findings may apply to the tropospheric particulate matter.

We have investigated particles with dry diameters in the size range from 12 to 67 μm. While these particles display the common efflorescence−deliquescence hysteresis of the inorganic fraction, liquid−liquid phase separation occurred with no observable hysteresis for all particle sizes. This indicates that the limits of metastability and instability are very close together in terms of RH. We therefore believe that liquid−liquid phase separation should occur readily also in submicrometer particles.

For the investigated size range, the particle morphologies showed the following size dependence: particles with liquid−liquid phase separation by spinodal decomposition and subsequent AS satellite formation in the outer phase showed a decrease to zero of the number of AS satellite inclusions for sizes below ~24 μm. For particles with liquid−liquid phase separation by nucleation and growth, the number of nucleation events decreased with decreasing particle size to one (e.g., 12 μm dry diameter for the 8:1 PEG-400/AS ratio). No size dependence of the morphology was observed for particles with AS dry mass fraction $x_{AS} > 0.65$. The outer phase grew at the surface of the particle with no satellite inclusions. Consequently, smaller particles presented only one inner phase (aqueous AS) surrounded by the outer phase (aqueous PEG-400) for all the investigated ratios of PEG-400/AS. Due to the contact with the surface, the two liquid phases can adopt different arrangements in the deposited droplets (see Appendix A). However, for submicrometer particles suspended in the air, we expect that the particle morphology will always be a sphere in a sphere, with the organic phase at the surface and without the formation of satellite inclusions. In the absence of large fractions of surfactants, more complex morphologies are thermodynamically not favored because the interfacial energy of a system increases with increasing interfacial area and with increasing curvature of the interfacial area (Kelvin effect).

The composition of tropospheric aerosol is more complex than the system that we have investigated, with a large number of different organics. Marcolli et al.[7] showed that an increase of the number of organic components decreases their DRH and may also decrease the DRH of inorganic components. When the organic fraction covers a large variety from hydrophilic to rather hydrophobic compounds, we expect that two liquid phases will be present in the particles over a large RH range.

These results are representative for a warm atmosphere. At very low atmospheric temperatures the organic fraction becomes more viscous or even glassy,[45] which might influence the phase separation kinetics and particle morphologies altogether.

7. Conclusions

We have shown that optical microscopy together with micro-Raman spectroscopy can be used to investigate the phases and phase transitions of micrometer sized particles as a function of relative humidity. The use of micro-Raman spectroscopy allows identification of the chemical composition of the liquid and solid phases that can be directly observed with an optical microscope. For the PEG-400/AS system, the $\nu_s(SO_4^{2-})$ and $\nu(CH_2)$ peaks prove to be the most important features of the Raman spectra to provide evidence on the mixing of the components at different RHs.

This work brings clear proof of liquid−liquid phase separation in micrometer sized particles containing partially immiscible components. We identify two pathways to attain a two-liquid-phases state in the mixed PEG-400/AS particles: (1) deliquescence of AS into a separated inner aqueous phase when the RH above the particle was increased and (2) separation of one liquid phase in two liquid phases when the RH above the particle was decreased. The kinetics of phase separation depend on particle size, the ratio of PEG-400/AS, surface tension effects, and diffusion of AS sulfate ions and inclusions. These all contribute to the observed morphologies of two-liquid-phases particles upon drying. In dependence upon the organic-to-inorganic ratio, OIR (i.e., PEG-400 to AS dry mass), phase separation is observed to occur by fundamentally different mechanisms, namely, nucleation-and-growth (OIR = 8:1 to 2:1), spinodal decomposition (OIR = 1.5:1 to 1:1.5) and growth of a second phase at the surface of the particle (OIR = 1:2 to 1:8).

Applying these findings to atmospheric conditions leads us to speculate that submicrometer sized organic/inorganic mixed aerosol particles may show frequently a core−shell structure with an inner inorganic and an outer organic phase, but without satellite inclusions as in the laboratory experiments.

Further research, using the same experimental techniques, will have to focus on characterizing the phases and phase transitions of more complex systems, such as mixed SOA−inorganic salts (ammonium sulfate, sodium chloride, ammonium nitrate) systems. The main goal will be to probe the RH conditions and the chemical composition (the ratio of organic-to-inorganic fraction) under which liquid−liquid phase separation occurs in such mixed particles.

Acknowledgment. This work was supported by Swiss National Foundation under contract No. 200020-103651/1. We would like to thank Alessandro Zardini for providing additional experimental data.

Appendix A. Hygroscopicity of Mixed PEG-400/AS Particles

Raman spectroscopy has been previously employed for describing the hygroscopic properties of mixed particles—such as $Ca(NO_3)_2/CaCO_3$[46] and ammonium sulfate-adipic acid[47]—deposited on a hydrophobic substrate. In both studies the

contribution of a second component (e.g., $CaCO_3$ and adipic acid) to the water uptake was neglected. In the PEG-400/AS system two liquid phases are present and PEG-400 also contributes to the water uptake of the particles.[18] Therefore, a quantification of the water content during drying and humidifying conditions by Raman spectroscopy is not feasible without knowledge of the volume ratio of the two phases. In this study we tried a different approach to estimate the hygroscopic growth factors (GFs) of the mixed PEG-400/AS particles, based on the shape of the deposited particles. To validate our calculations, we compare the GFs with the GFs predicted with the Zdanovskii−Stokes−Robinson approach.

A.1. Shape of Deposited Particles. With the present experimental setup, the optical microscope gives only the top view of the particles, but no direct information on the side view. To test whether or not the GFs of the mixed PEG-400/AS particles can be estimated with our setup and to determine how the substrate may influence the distribution of the two liquid phases within the deposited particles, we attempt a reconstruction of the particle shape. For this purpose we used the radius of inner and outer liquid phases, the volume ratio of the two liquid phases—determined for bulk solutions as a function of RH—and contact angle measurements from side views of larger PEG-400/AS droplets (1−3 μL) deposited on the hydrophobically coated surface of the microscope slide. The contact angles measured for 19:1 and 1:19 ratios (by weight) of PEG-400/AS droplets at the two-liquid-phases/one-liquid-phase boundary (~90% RH) are 52 ± 3° and 52 ± 2°, respectively, whereas for AS saturated droplets the contact angle is 83 ± 5°. Using these values, we calculated the droplet's height, and the AS to total volume ratio assuming different arrangements of the two immiscible liquid phases in the particle. Figure 9 shows the changes of the ratio of the inner phase volume (V_{AS}) and total volume (V_{tot}) as a function of RH for the arrangements of the two liquid phases in the particle as outlined in Figure 10. By comparing the ratio of V_{AS}/V_{tot} in micrometer-sized particles and in bulk solutions, we can attribute certain morphologies to the deposited particles. For example, in a PEG-400/AS particle with OIR = 1:1 the two liquid phases form most likely spherical calottes of the same height (Figure 10c), with contact angles of 52° and 73 ± 2° for the outer and inner calotte, respectively. For this arrangement, the contact angle calculated for the inner calotte is lower than the one of the AS saturated droplet because the dimension of the inner phase is restrained by the height of the particle. For a particle with OIR = 1.5:1 the volume ratio is compatible with a half-sphere in a spherical calotte with contact angle 52°. Because the volume of the inner phase is lower than in the previous case, the particle is high enough so that the aqueous AS phase can adopt a higher contact angle, thus reducing the interfacial area of the hydrophilic phase with the substrate. For particles with OIR = 8:1, there are two morphologies that are similarly close to the bulk measurements, namely, half spheres in a spherical calotte (contact angle 52°) and spheres in a spherical calotte (contact angle 52°). On the basis of this analysis, we can therefore not differentiate between aqueous AS inclusions in contact with the hydrophobic surface and those fully immersed in the volume of the droplet. For particles with OIR = 1:2 there is no calotte in a calotte arrangement that gives a V_{AS}/V_{tot} close to the bulk measurements. A morphology that is consistent with the bulk measurements is half ellipsoid in a spherical calotte with a 52° contact angle (see Figure 10d). One dimension of the half-ellipsoid is equal to the height of the particle, and the other two dimensions are equal to the radius of the inner phase. Because we suppose that the contact angle controls the height of the particle, the inner phase, has to adapt its shape to fit into the spherical calotte with the 52° contact angle.

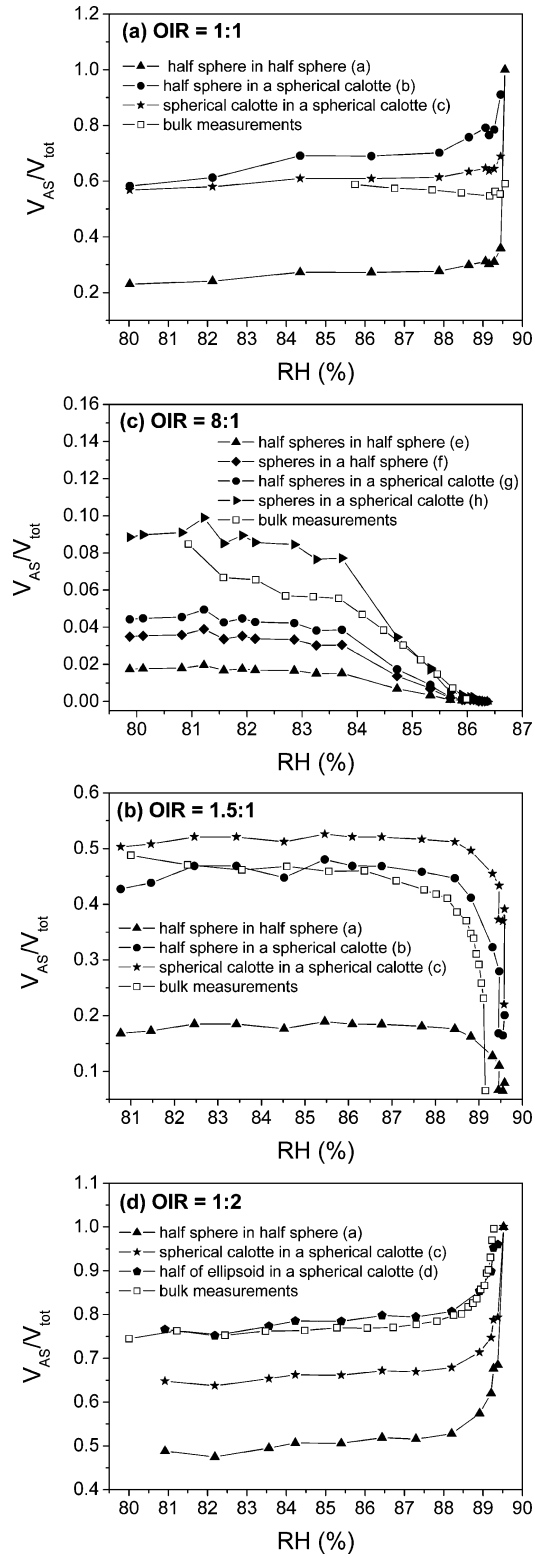

Figure 9. Ratio of AS phase volume to the total volume (V_{AS}/V_{tot}) from bulk measurements and for different particle morphologies, as illustrated in Figure 10.

Particles and bulk solutions show similar behavior regarding the evolution of AS and PEG-400 phase volumes with increasing RH. Although for all compositions the V_{AS}/V_{tot} is almost constant, when RH approaches the one liquid phase boundary

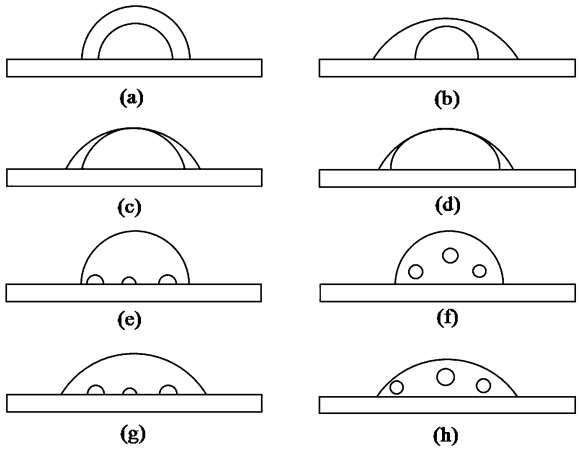

Figure 10. Possible arrangements of the aqueous AS and PEG-400 phases within the deposited droplet: (a) half-sphere in half-sphere; (b) half-sphere in a spherical calotte (contact angle 52°); (c) spherical calotte in a spherical calotte (same height; contact angle of outer spherical calotte 52°); (d) half-ellipsoid in a spherical calotte (same height; contact angle of outer spherical calotte 52°). For the 8:1 PEG-400/AS particle the following arrangements have been considered: (e) half spheres in half sphere; (f) spheres in half sphere; (g) half spheres in a spherical calotte (contact angle 52°); (h) spheres in a spherical calotte (contact angle 52°).

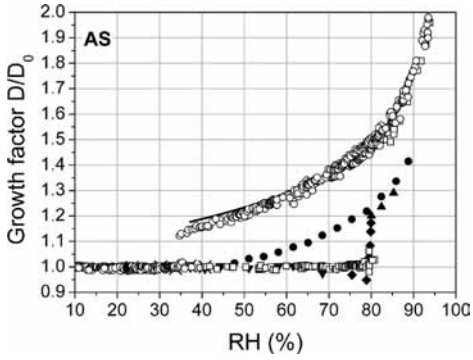

Figure 11. Humidity cycles for pure AS particles. Decreasing RH: ●, liquid; ×, solid. Increasing RH: ▼, solid; ◆, uptake of water; ▲, liquid. Symbols for Sjogren et al.: □, hydration PSI; ○, dehydration PSI; —, ZSR theory.

different behavior is observed for OIR = 1:1 and 1:2, namely, an increase in the AS phase volume, whereas a decrease is observed for OIR = 8:1 and 1.5:1.

A.2. Water Uptake and Release during Humidity Cycle. To verify whether the GFs of the deposited particles can be estimated with the present setup, we calculated the GF using the wet and dry diameter (measured at ~10% RH) with the assumption of a constant contact angle for the whole RH range. Therefore, the changes in diameter to height during the cycles are not captured in our calculation. As a first step we compare the GF of pure AS with the results obtained in field measurements, e.g., by the hygroscopic tandem differential mobility analyzer (HTDMA) technique. During HTDMA measurements, spherical particles grow equally in all directions whereas the apparent growth in height and growth in diameter of particles deposited on a substrate may differ. The comparison of GFs measured in this study with HTDMA results from Sjoegren et al.[48] gives therefore an indication on how the particles on the substrate grow and shrink during humidity cycles. Figure 11 shows the hygroscopic GF for pure AS as a function of RH compared with the HTDMA measurements. Pure AS particles deposited on a substrate show a lower apparent growth than AS aerosols in HTDMA measurements. This is likely due to a stronger growth in height than in diameter of the deposited particles yielding the apparently lower water uptake. This implies that the contact angle increases during water uptake and decreases when water is released. Interestingly, AS particles show no real efflorescence step (Figure 11), indicating that water loss during crystallization is not accompanied by a reduction of the particle's diameter but rather its height. Compaction occurs during water uptake, leading to shrinkage of the particle's diameter. However, for mixed PEG-400/AS particles shrinkage of particle diameter was observed when AS effloresced. Because no HTDMA data are available for this system, we compare the GFs of mixed PEG-400/AS particles with the GFs calculated according to the Zdanovskii−Stokes−Robinson approach[49,50] using the following formula:

$$\mathrm{GF}_{\mathrm{mixed}} = \left(\sum_k \varepsilon_k \mathrm{GF}_k^3\right)^{1/3} \qquad \text{(A.2.1)}$$

where ε represents the volume fraction of the components in the dry particle and the GFs are the GFs of the pure components. We used for AS the GF parametrized by Sjogren et al.[48] whereas the GF of PEG-400 was derived from EDB measurements.[18] The mass GF was converted to a volume GF that was used to determine the diameter GF as follows:

$$\mathrm{GF} = \left(\frac{m(\mathrm{RH})\rho_0}{m_0\rho(\mathrm{RH})}\right)^{1/3} \qquad \text{(A.2.2)}$$

where m_0 and ρ_0 are the initial particle mass and density at dry conditions (we used 1.1254 g/cm^3 for the density of pure PEG-400) and m(RH) and ρ(RH) are the mass and the density of the particle depending on the RH. The ρ(RH) was parametrized between 30−95% RH using the bulk data, with the assumption of additive volumes ($\rho(\mathrm{RH}) = a + b\cdot\mathrm{RH} + c\cdot\mathrm{RH}^2 + d\cdot\mathrm{RH}^3$, where RH is given in percent and the coefficients a, b, c, and d were fitted as +1.1473, −0.00159, +2.79905 × 10^{-5} and −2.37842 × 10^{-7}, respectively).

Figure 12 shows the humidity cycles for PEG-400/AS particles with OIR = 1:1, 1:2, and 8:1 as a function of RH at ~293 K. Each panel shows for each composition the humidity cycles of three particles, with data for the first particle given in detail (with indication of the observed liquid and solid phases). The cycles all start and end at high RH. The GFs at 80% RH (when AS is totally deliquesced) decrease with increasing fraction of PEG-400 from 1.45−1.42 for OIR = 1:2 to 1.07−1.05 for OIR = 8:1. The comparison between particles with the same composition shows differences in GF of up to 15%. We assume that the overall water uptake of all particles is similar and that the observed differences represent the variability in contact angle. At the end of the cycle, most humidity curves reach again a value close to the original GF, indicating the reversibility of the changes in particle morphology during hygroscopic growth and evaporation.

The Zdanovskii−Stokes−Robinson (ZSR) mixing rule was used to predict GFs using the GFs of the components in pure form. The ZSR GFs for the drying branch are shown in Figure 12 for mixed particles with OIR = 1:1, 1:2, and 8:1. For 1:1 mixed PEG-400/AS particles the ZSR curve is higher at high RH, but as RH decreases, it approaches the experimental curves. These differences can be attributed to the way the particles grow and shrink. Changes in the composition of the particles, due to water release or uptake, may also change the contact angle and

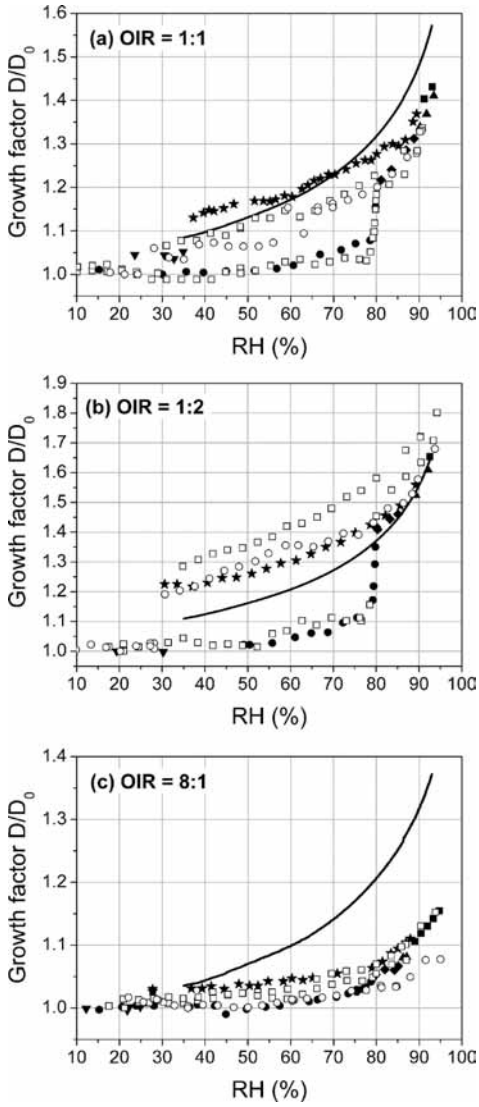

Figure 12. Humidity cycles for mixed PEG-400/AS with OIR 1:1, 1:2, and 8:1. Each panel shows data of three particles. Symbols for the first particle: ■, one liquid phase decreasing RH; ★, two liquid phases decreasing RH; ▼, solid and liquid decreasing RH; ●, solid and liquid increasing RH; ◆, two liquid phases increasing RH; ▲, one liquid phase increasing RH. Other symbols: □, second particle; ○, third particle; —, ZSR mixing rule.

therefore the height of the particle. The particles with a 1:2 PEG-400/AS ratio show good agreement with the ZSR curve at higher RH and higher GFs at lower RH. For this case it seems that water release is accompanied by stronger shrinkage in particle height than in diameter. For the 8:1 PEG-400/AS particles, there was no significant change in the diameter of the particles observed in the microscope. In this case the particles seem to grow and shrink mainly in height and to retain almost the original diameter during the whole cycle. As a consequence, the experimental and the ZSR curve do not meet.

To summarize, whether water release and uptake leads to changes of the particle's diameter or height seems to depend on the ratio of PEG-400 to AS. Particles change more in diameter when AS is the predominant component and very little when a low amount of AS is present. We conclude that with the present experimental setup, an accurate prediction of the GFs of deposited particles is not possible when assuming a constant contact angle.

Appendix B. Movies of PEG-400/AS Particles

Three movies showing liquid−liquid phase separation in mixed PEG-400/AS particles with OIR = 1:1, 8:1, and 1:2 can be downloaded. The movies are sped up after the first stages of the liquid−liquid phase separation.

Movie 1 shows liquid−liquid phase separation via spinodal decomposition and AS efflorescence in the mixed PEG-400/AS particle with OIR = 1:1; shown in Figure 2a.

Movie 2 shows liquid−liquid phase separation via nucleation-and-growth, AS efflorescence and deliquescence, and one liquid phase formation in the mixed PEG-400/AS particle with OIR = 8:1; shown in Figure 2b.

Movie 3 shows liquid−liquid phase separation by growth of a second phase at the surface of the particle and AS efflorescence in the mixed PEG-400/AS particle with OIR = 1:2; shown in Figure 2c.

References and Notes

(1) Colberg, C. A.; Luo, B. P.; Wernli, H.; Koop, T.; Peter, Th. *Atmos. Chem. Phys.* **2003**, *3*, 909–924.
(2) Martin, S. T. *Chem. Rev.* **2000**, *100*, 3403–3453.
(3) Ravishankara, A. R. *Science* **1997**, *276*, 1058.
(4) Hallquist, M.; Stewart, D. J.; Stephenson, S. K.; Cox, R. A. *Phys. Chem. Chem. Phys.* **2003**, *5*, 3453–3463.
(5) Mozurkewich, M.; Calvert, J. G. J. *Geophys. Res.* **1988**, *93* (D12), 15889–15896.
(6) Erdakos, G. B.; Pankow, J. F. *Atmos. Environ.* **2004**, *38*, 1005–1013.
(7) Marcolli, C.; Luo, B. P.; Peter, Th. *J. Phys. Chem. A* **2004**, *108*, 2216–2224.
(8) Salcedo, D. *J. Phys. Chem. A* **2006**, *110*, 44, 12158−12165.
(9) Kanakidou, M.; Seinfeld, J. H.; Pandis, S. N.; Barnes, I.; Dentener, F. J.; Facchini, M. C.; Van Dingenen, R.; Ervens, B.; Nenes, A.; Nielsen, C. J.; Swietlicki, E.; Putaud, J. P.; Balkanski, Y.; Fuzzi, S.; Horth, J.; Moortgat, G. K.; Winterhalter, R.; Myhre, C. E. L.; Tsigaridis, K.; Vignati, E.; Stephanou, E. G.; Wilson, J. *Atmos. Chem. Phys.* **2005**, *5*, 1053–1123.
(10) Decesari, S.; Facchini, M. C.; Fuzzi, S.; Tagliavini, E. *J. Geophys. Res.* **2000**, *105* (D1), 1481–1489.
(11) Saxena, P.; Hildemann, L. M. *J. Atmos. Chem.* **1996**, *24*, 57–109.
(12) Braban, C. F.; Abbatt, J. P. D. *Atmos. Chem. Phys.* **2004**, *4*, 1451–1459.
(13) Brooks, S. D.; Wise, M. E.; Cushing, M.; Tolbert, M. A. *Geophys. Res. Lett.* **2002**, *29* (19), 1917.
(14) Brooks, S. D.; Garland, R. M.; Wise, M. E.; Prenni, A. J.; Cushing, M.; Hewitt, E.; Tolbert, M. A. *J. Geophys. Res.* **2003**, *108* (D15), 4487.
(15) Parsons, M. T.; Knopf, D. A.; Bertram, A. K. *J. Phys. Chem. A* **2004**, *108*, 11600–11608.
(16) Badger, C. L.; George, I.; Griffiths, P. T.; Braban, C. F.; Cox, R. A.; Abbatt, J. P. D. *Atmos. Chem. Phys.* **2006**, *6*, 755–768.
(17) Choi, M. Y.; Chan, C. K. *Environ. Sci. Technol.* **2002**, *36*, 2422–2428.
(18) Marcolli, C.; Krieger, U. K. *J. Phys. Chem. A* **2006**, *110*, 1881–1893.
(19) Pankow, J. F. *Atmos. Environ.* **2003**, *37*, 3323–3333.
(20) Buajarern, J.; Mitchem, L.; Reid, J. P. *J. Phys. Chem. A* **2007**, *111*, 9054–9061.
(21) Graber, E. R.; Rudich, Y. *Atmos. Chem. Phys.* **2006**, *6*, 729–753.
(22) Petters, M. D.; Kreidenweis, S. M.; Snider, J. R.; Koehler, K. A.; Wang, Q.; Prenni, A. J.; Demott, P. J. *Tellus* **2006**, *58B*, 196–205.
(23) Albertsson, P. A. *Partition of Cell Particles and Macromolecules*; Wiley-Interscience: New York, 1971.
(24) Zaslavsky, B. Y. *Aqueous Two-Phase Partitioning: Physical Chemistry and Bioanalytical Applications*; Marcel Dekker: New York, 1995.
(25) Shelby, J. E. *Introduction to Glass Science and Technology*; The Royal Society of Chemistry: Cambridge, U.K., 1997.
(26) Cahn, J. W. *Acta Metall.* **1961**, 9.
(27) Egry, I.; Herlach, D.; Kolbe, M.; Ratke, L.; Reutzel, S.; Perrin, C.; Chatain, D. *Adv. Eng. Mater.* **2003**, *5* (11), 819–823.
(28) Papon, P.; Leblond, J.; Meijer, P. H. E. *The Physics of Phase Transitions: Concepts and Applications*, Springer, 1999.
(29) Smith, A. P.; Douglas, J. F.; Amis, E. J.; Karim, A. *Langmuir* **2007**, *23* (24), 12380–12387.
(30) Wang, S. J.; Wu, C. J.; Ren, M.-Q.; Van Horn, R. M.; Graham, M. J.; Han, C. C.; Chen, E. Q.; Cheng, S. Z. D. *Polymer* **2009**, *50* (4), 1025–1033.

(31) Settles, G. S. *Schlieren and shadowgraph techniques: visualizing phenomena in transparent media*; Springer, New York, 2001; p 376; ISBN 3540661557, 9783540661559.

(32) Han, H. Z. Y.; Lee, S. S.; Manson, J. A. E.; Hilborn, J. G. *Appl. Spectrosc.* **2000**, *54* (6), 783–794.

(33) Knopf, D. A. Thermodynamic Properties and Nucleation Processes of Upper Tropospheric and Lower Stratospheric Aerosol Particles, Diss. ETH No. 15103, 2003.

(34) Di Noto, V.; Bettinelli, M.; Furlani, M.; Lavina, S.; Vidali, M. *Macromol. Chem. Phys.* **1996**, *197*, 375–388.

(35) Matsuura, H.; Miyazawa, T. *Bull. Chem. Soc. Jpn.* **1968**, *8*, 1798–1808, 41.

(36) Dong, J.-L.; Li, X.-H.; Zhao, L.-J.; Xiao, H.-S.; Wang, F.; Guo, X.; Zhang, Y.-H. *J. Phys. Chem. B* **2007**, *111*, 12170–12176.

(37) Colberg, C. A. *Experimente an levitierten $H_2SO_4/NH_3/H_2O$-Aerosolteilchen: Atmosphaerische Relevanz von Letovizit*, DISS. ETH, No. 14331, 2001.

(38) Xu, J.; Imre, D.; McGraw, R.; Tang, I. *J. Chem. Phys. B* **1998**, *102*, 7462–7469.

(39) Lewis, E. R. *Aerosol Sci.* **2006**, *37*, 1605–1617.

(40) Assovskii, I. G.; Rashkovskii, S. A. *Dokl. Phys. Chem.* **2002**, *385*, 149–153 (Engl. Transl.). *Dokl. Akad. Nauk* **2002**, *385*, 75−79.

(41) Jackson, K. A. *Kinetic processes: Crystal Growth, Diffusion and Phase Transition in Materials*; John Wiley & Sons: New York, 2004; p 13.

(42) Wishaw, B. F.; Stokes, R. H. *J. Am. Chem. Soc.* **1954**, *76* (8), 2065–2071.

(43) Bentz, D. P.; Snyder, K. A.; Cass, L. C.; Peltz, M. A. *Cement Concrete Comp.* **2008**, *30*, 674–678.

(44) Ottani, S.; Vitalini, D.; Comelli, F.; Castellari, C. *J. Chem. Eng. Data* **2002**, *47* (5), 1197–1204.

(45) Zobrist, B.; Marcolli, C.; Pedernera, D. A.; Koop, T. *Atmos. Chem. Phys.* **2008**, *8*, 5221–5244.

(46) Liu, Y. J.; Zhou, T.; Zhao, D. F.; Zhang, Z. F. *Atmos. Chem. Phys.* **2008**, *8*, 7205–7215.

(47) Yeung, M. C.; Lee, A. K. Y.; Chan, C. K. *Aerosol Sci. Technol.* **2009**, *43*, 387–399.

(48) Sjogren, S.; Gysel, M.; Weingartner, E.; Baltensperger, U.; Cubison, M. J.; Coe, H.; Zardini, A. A.; Marcolli, C.; Krieger, U. K.; Peter, T. *J. Aerosol Sci.* **2007**, *38*, 157–171.

(49) Zdanovskii, A. B. Novyi metod rascheta rastvorimostei elektrolitov v mnogokomponentnykh sistemakh 1,2. *Zh. Fiz. Khim.* **1948**, *22*, 1486–1495, 1478−1485.

(50) Stokes, R. H.; Robinson, R. A. *J. Phys. Chem.* **1966**, *70, 7*, 2126–2131.

JP905054D